Crystal Structure of the Ascorbate Peroxidase−Salicylhydroxamic Acid Complex[†]

Katherine H. Sharp,[‡] Peter C. E. Moody,[§] Katherine A. Brown,[||] and Emma Lloyd Raven*,[‡]

Department of Chemistry, University of Leicester, University Road, Leicester LE1 7RH, U.K., Department of Biochemistry, University of Leicester, University Road, Leicester LE1 7RH, U.K., and Department of Biological Sciences, Centre for Molecular Microbiology and Infection, Flowers Building, Imperial College London, London SW7 2AZ, U.K.

Received April 5, 2004; Revised Manuscript Received May 4, 2004

ABSTRACT: Ascorbate peroxidase is a bifunctional peroxidase that catalyzes the H_2O_2-dependent oxidation of both ascorbate and various aromatic substrates. The ascorbate binding site was recently identified as being close to the γ-heme edge [Sharp, K. H., Mewies, M., Moody, P. C. E., and Raven, E. L. (2003) *Nat. Struct. Biol. 10*, 303−307]. In this work, the X-ray crystal structure of recombinant soybean cytosolic ascorbate peroxidase (rsAPX) in complex with salicylhydroxamic acid (SHA) has been determined to 1.46 Å. The SHA molecule is bound close to the δ-heme edge in a cavity that connects the distal side of the heme to the surface of the protein. There are hydrogen bonds between the phenolic hydroxide of the SHA and the main chain carbonyl of Pro132, between the carbonyl oxygen of SHA and the side chain guanadinium group of Arg38, and between the hydroxamic acid group and the indole nitrogen of Trp41. The structure provides the first information about the location of the aromatic binding site in ascorbate peroxidase and, together with our previous data [Sharp, K. H., et al. (2003) *Nat. Struct. Biol. 10*, 303−307], completes the structural description of the binding properties of ascorbate peroxidase. The mechanistic implications of the results are discussed in terms of our current understanding of how APX catalyzes oxidation of different types of substrates bound at different locations.

The heme peroxidase enzymes (reviewed in refs *1*−*4*) catalyze the H_2O_2-dependent oxidation of a wide variety of substrates, in most cases small organic substrates. They have been classified on the basis of sequence homology (*5*) into three types. Class I heme peroxidases contain the prokaryotic enzymes, including cytochrome *c* peroxidase (CcP),[1] ascorbate peroxidase (APX), and the gene-duplicated bacterial catalase-peroxidases. Class II contains the fungal peroxidase enzymes, including manganese peroxidase and lignin peroxidase. Class III contains the classical secretory peroxidases, the most notable example being horseradish peroxidase (HRP). Mechanistically, these enzymes are very well characterized; they share a common catalytic cycle that involves formation of a two equivalent oxidized intermediate, known as Compound I, followed by reduction of Compound I by substrate (eqs 1−3, where P is peroxidase, HS is the substrate, and $S^{\bullet}$ is the one-electron oxidized form of the substrate).

$$P + H_2O_2 \rightarrow \text{Compound I} + H_2O \quad (1)$$

$$\text{Compound I} + HS \rightarrow \text{Compound II} + S^{\bullet} \quad (2)$$

$$\text{Compound II} + HS \rightarrow P + S^{\bullet} + H_2O \quad (3)$$

Much of the structure−function work (*1*−*4*, *6*−*8*) on the heme peroxidases has focused on Compound I formation (eq 1), and a consistent picture of this step has emerged: the peroxidases have very similar heme active site structures that, in all cases, have been designed to support formation of the high valent Compound I intermediate. In contrast, the identity of the substrate (eqs 2 and 3) varies enormously (it can be a metal ion, an organic/phenolic substrate, or a protein molecule), and it is this variety in substrate specificity, and not Compound I formation, that delivers the rich diversity of function across the peroxidase family. It follows that to understand biological function, we need an experimental framework that allows detailed rationalization of substrate binding.

On the whole, however, our understanding of the structural features that define substrate specificity in the heme peroxidase enzymes is poorly developed compared to our understanding of Compound I formation. This is in part because structural information for peroxidase−substrate complexes has been slower to emerge (*9*−*17*), but is also because, in

[†] This work was supported by The Wellcome Trust (Grant 063688/Z/01/Z to E.L.R.), the Engineering and Physical Sciences Research Council, and The Institute of Applied Catalysis (studentship to K.H.S.).

* To whom correspondence should be addressed. Telephone: +44 (0)116 252 2099. Fax: +44 (0)116 252 2789. E-mail: emma.raven@le.ac.uk.

[‡] Department of Chemistry, University of Leicester.

[§] Department of Biochemistry, University of Leicester.

[||] Imperial College London.

[1] Abbreviations: APX, ascorbate peroxidase; rsAPX, recombinant soybean cytosolic ascorbate peroxidase; SHA, salicylhydroxamic acid (2-hydroxybenzhydroxamic acid); BHA, benzyhydroxamic acid; CcP, cytochrome *c* peroxidase; HRP, horseradish peroxidase; ARP, *A. ramosus* peroxidase.

10.1021/bi049343q CCC: $27.50
Published on Web 06/18/2004

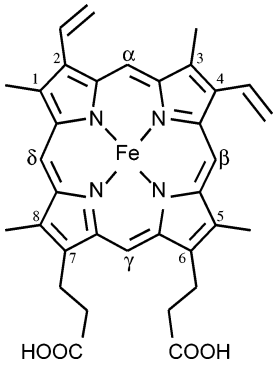

FIGURE 1: Structure of iron protoporphyrin IX, showing the nomenclature used in this work. This nomenclature is consistent with that used in our previous work (*26*).

some cases (*9*, *12*), the substrate is atypical and has not, therefore, provided the necessary generic insight. A lack of comparative substrate binding information, to allow connections to be made between different peroxidases, has also been prohibitive.

Within this wider framework, it was recently realized that ascorbate peroxidase (APX), which catalyzes the H_2O_2-dependent oxidation of ascorbate (*18*−*20*), has structural, functional, and substrate binding properties that places it at an important interface between peroxidases [a distinction that has been highlighted recently (*21*)]. Hence, the sequence of APX is highly identical with the most prominent and well-characterized class I peroxidase, CcP, as well as with the bacterial catalase-peroxidases. In addition to ascorbate, APX is also able to catalyze the oxidation of a variety of aromatic substrates [e.g., *p*-cresol, guaiacol, pyrogallol, *o*-dianisidine, and 2,2′-azinobis(3-ethylbenzothiazoline-6-sulfonic acid) (ABTS)] that are typical of the class II and class III peroxidases (*21*, *22*). In some cases, oxidation of these aromatic substrates is faster than oxidation of ascorbate itself (*18*), and it is likely that this is linked to a physiological role, since there are high levels of phenolic compounds present *in planta*. Altogether, the close sequence identity to CcP coupled with its bifunctional substrate specificity that mimics that of the class II and III peroxidases makes APX an exceptionally useful comparative model for our general understanding of substrate binding because it provides an overarching framework that encompasses many features that have, so far, only been found separately.

It is only recently that detailed information about substrate binding in APX has appeared. The hypothesis that has emerged is as follows (*23*−*25*). There are two, separate substrate binding locations. The first, close to the γ-meso (C15) position of the heme (Figure 1), is utilized by ascorbate; the second is used primarily by aromatic substrates (*23*), but its location is not known. We have recently determined the crystal structure of recombinant soybean cytosolic APX (rsAPX) in complex with ascorbate (*26*). The structure has confirmed the γ-heme edge as the primary site of oxidation of ascorbate and provides the first comparative rationalization of the different substrate specificities of APX and CcP. In this work, we have identified the second, aromatic binding site by determining the crystal structure of rsAPX in complex with salicylhydroxamic acid (SHA, Figure 2). Together with our previous data (*26*), this now provides a complete description of substrate binding in APX.

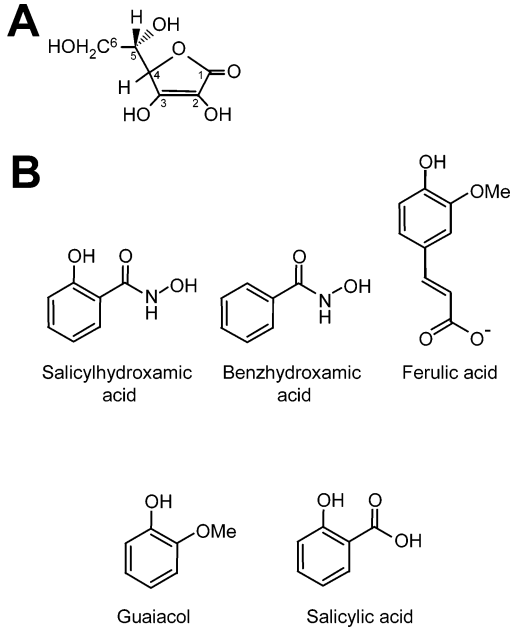

FIGURE 2: (A) Structure of ascorbic acid. The pK_a values of the 2-OH and 3-OH groups are 11.3 and 4.0, respectively (*42*). (B) Structures of the various aromatic compounds discussed in this paper. Salicylhydroxamic acid contains two acidic protons on the phenolic [pK_a = 9.8 (*33*)] and hydroxamic acid [pK_a = 7.4 (*33*)] groups.

EXPERIMENTAL PROCEDURES

Protein Purification and Preparation of Crystals. Recombinant soybean cytosolic APX (rsAPX) was prepared from *Escherichia coli* SG1300 (pREP4) by incorporation of a pQE30-derived expression vector and purified as described previously (*27*). The final elution from the Ni^{2+}−nitrilotriacetic acid agarose column (Qiagen) was carried out using pH (4.2) rather than using imidazole, and the heme reconstitution step was carried out and then left overnight rather than over 15 min as described. Samples prepared in this way eluted as a single band by SDS−PAGE and by FPLC using a Superdex 75 HR 10/30 column. Purity was also assessed using the ratio of absorbancies at the Soret and 280 nm peaks. For rsAPX, samples with an A_{407}/A_{280} of greater than 2.0 were considered pure. Samples (≈20 mg/mL) were stored in deionized water in 50 μL aliquots. Enzyme concentrations were determined using the molar absorption coefficient for rsAPX [ϵ_{407} = 107 mM^{-1} cm^{-1} (*27*)]. Samples of rsAPX were assayed (100 mM phosphate at pH 7.0 and 25.0 °C) against guaiacol using established protocols (*27*) and using an ϵ_{470} of 22.6 mM^{-1} cm^{-1} (*28*). Data were fitted to the Michaelis−Menten equation.

Crystals of rsAPX were prepared as described previously (*26*). The best crystals grew to ∼150 μm in length and 75 μm in cross section. Guaiacol is too insoluble in water for sufficiently high concentrations to be obtained in solution for soaking into rsAPX crystals. Guaiacol is soluble in EtOH or MeOH, but attempts to soak it (at various concentrations in EtOH or MeOH) into the crystals resulted in cracking of the crystals under all conditions that were attempted. Solubility can be improved by functionalization of the methoxy group with the (more hydrophilic) hydroxamic acid group. In this case, it was possible to obtain crystals of the rsAPX−SHA complex by soaking the crystals in a mother

Table 1: Data Collection and Refinement Statistics for the rsAPX−SHA Complex[a]

data collection	
resolution range (outer bin) (Å)	50−1.46 (1.51−1.46)
total no. of observations	310054
no. of unique reflections	43221
$I/\sigma I$	32.2 (3.4)
R_{merge} (%)	7.6
completeness (%)	99.2
refined structure	
R_{work} (R_{free})	0.155 (0.185)
rms deviations from ideal	
bonds (Å)	0.011
angles (deg)	1.344

[a] The crystal cell dimensions are as follows: $a = b = 82.77$ Å, $c = 74.99$ Å. The space group is $P4_22_12$. Refined coordinates and structure factors have been deposited with the Protein Data Bank (*51*) as entry 1VOH.

liquor solution containing 100 mM SHA (Aldrich, 99.0%) for approximately 1 min. The SHA was dissolved by adding 1 M sodium hydroxide to the mother liquor to adjust the pH to ~10. The pH was then returned to 8.3 by adding hydrochloric acid.

Equilibrium Binding Constants. Equilibrium dissociation constants, K_d (100 mM potassium phosphate at pH 8.3), for the binding of SHA to rsAPX were determined using electronic spectroscopy according to previously published procedures (*29*) by addition of known amounts of SHA to rsAPX (≈5 μM rsAPX). Additions of SHA were determined gravimetrically. Binding constants were determined from plots of fractional saturation versus free ligand concentration according to published procedures (*29*). On the basis of pH-dependent binding data, which show an increase in K_d with pH that corresponds with the pK_a of the SHA, it has been reported that only the neutral form of SHA binds (*30*−*32*). Binding of SHA to rsAPX was also found to be pH-dependent (not shown), and we have therefore corrected binding data for ionization [pK_a = 7.4 (*33*)] of the hydroxamic acid group of SHA, as previously described (*30*, *31*). Reported values for K_d are an average of at least two independent measurements.

Data Collection and Refinement. Diffraction data were collected for the rsAPX−SHA complex on beam-line ID14-4 at ESRF (Grenoble, France) using an ADSC Quantum-4 detector. Data to 1.46 Å were collected over a 90° rotation in 0.5° images. All data were collected at 100 K. Data collection statistics are shown in Table 1, and 5% of the data were flagged for the calculation of R_{free} and excluded from subsequent refinement. The structure was refined from a model derived from the 1.45 Å rsAPX−ascorbate complex (*26*) (Protein Data Bank entry 1OAF) by the removal of bound ligand and water molecules. Several cycles of refinement using REFMAC5 from the CCP4 suite (*34*) and incorporation of solvent molecules gave a model with a crystallographic *R*-factor for all data of 15.5% and an R_{free} of 18.5%. The electron density for SHA was clear and unambiguous; the structure was incorporated into the last cycles of refinement. XTALVIEW (*35*) was used throughout for manual adjustment, ligand fitting, and interpretation of water structure.

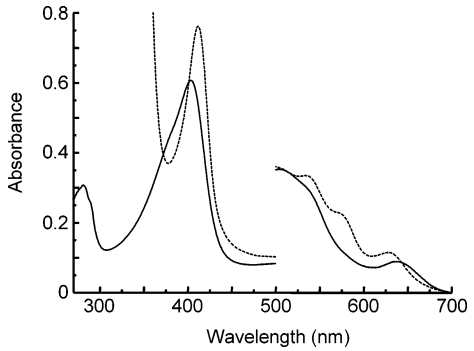

FIGURE 3: Electronic absorption spectra of rsAPX (—) and the rsAPX−SHA complex (- - -) (100 mM phosphate at pH 8.0). SHA absorbs strongly below 350 nm, and this spectrum has been truncated.

RESULTS

The UV−visible spectrum of rsAPX (λ_{max} = 407, 505, and 637 nm) and the rsAPX−SHA complex are shown in Figure 3. Addition of SHA leads to an increase in intensity and a red shift of the Soret band from 407 to 418 nm. New bands at 540, 580, and 630 nm appear. These changes are consistent with the formation of a predominantly six-coordinate heme derivative in the presence of SHA. A binding constant, K_d, of 8 ± 1 μM was determined for the rsAPX−SHA interaction (100 mM phosphate at pH 8.3) (data not shown). Binding of SHA to the heme will inhibit peroxidase activity by competing with H_2O_2, which is analogous to the binding of other strong ligands (e.g., cyanide). At high concentrations of SHA, the k_{cat} value for oxidation of guaiacol by rsAPX is only ≈50% of the value observed in the absence of SHA.[2] To establish whether binding of SHA is affected by the presence of other substrates, the binding constant, K_d, for SHA was determined in the presence of both ascorbate (25 mM) and guaiacol (25 mM). In this case, the K_d for SHA binding in the presence of guaiacol increases (K_d = 32 ± 2 μM), but the corresponding value in the presence of ascorbate does not change (K_d = 8 ± 1 μM) (data not shown), indicating that guaiacol and SHA compete for the same site but that ascorbate and SHA do not. When H_2O_2 is added to a solution of rsAPX and SHA, there is no decrease in the SHA peak at 300 nm, indicating that no oxidation occurs.

The overall structure of rsAPX in complex with SHA is shown in Figure 4. Comparison with the structure of the SHA-free enzyme (*26*) shows that binding of SHA leads to no major structural rearrangements of the enzyme (rms deviation in Cα positions of 0.21 Å). However, there is a slight adjustment of the side chain dihedral angle χ_2 of His42 with respect to that of the rsAPX structure (not shown). The electron density for the SHA molecule in the region of the heme group is unambiguous, allowing its position to be defined with precision (Figure 4). The SHA molecule is located in a cavity that connects the distal side of the heme to the surface of the protein. The mouth of the cavity is

[2] Competitive inhibition experiments with rsAPX and ascorbate−H_2O_2 in the presence of SHA were not carried out because SHA absorbs intensely at the wavelengths used for ascorbate assays (290 or 260 nm). The corresponding experiment with guaiacol showed a change in both K_M and k_{cat}. This may be due to the fact that both H_2O_2 and guaiacol are inhibited by SHA; these experiments were not pursued further, therefore.

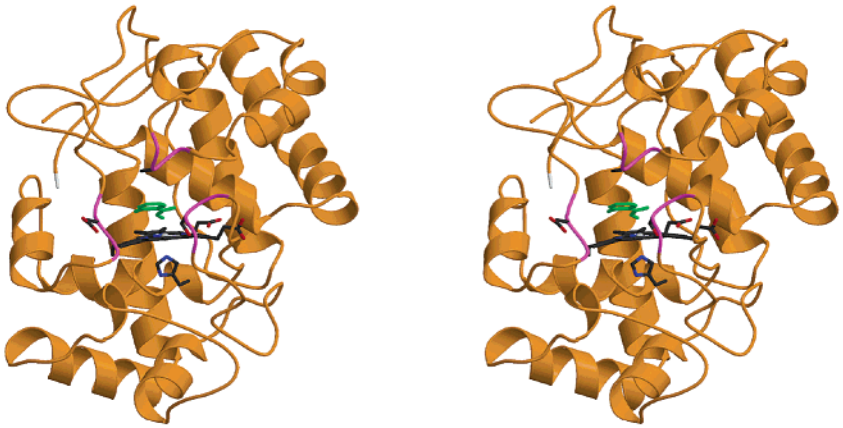

FIGURE 4: Stereo representation of the overall structure of the rsAPX−SHA complex, showing the heme with the proximal histidine residue in black and the bound SHA in green. The loops defining the mouth of the binding pocket are highlighted in magenta. The loop including Ala70 is shown directly above the SHA molecule; the loop including Asp133 is to the left of the SHA molecule, and the loop including Ser173 is to the right. The atoms of the side chains of Ala70, Asp133, and Ser173 are also shown. This figure was prepared using MOLSCRIPT (*48*) and RASTER3D (*49*).

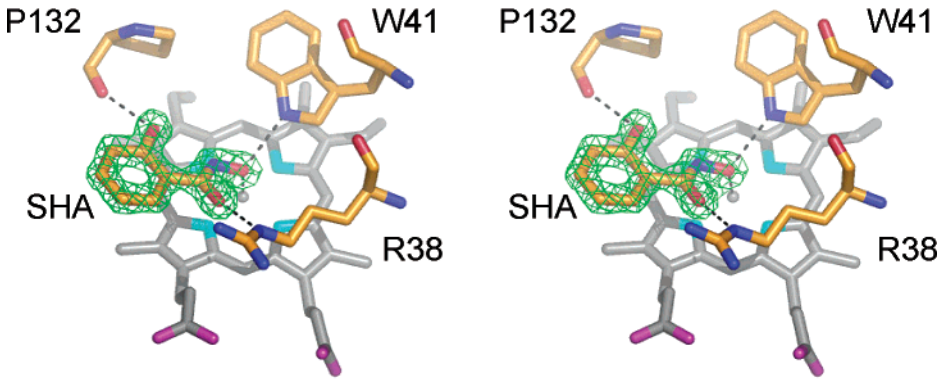

FIGURE 5: Stereoview of the rsAPX−SHA complex, showing the heme (gray) and the difference electron density (green) for the SHA. Hydrogen bonds are indicated by dashed lines (black). This figure was prepared using PyMOL (*50*).

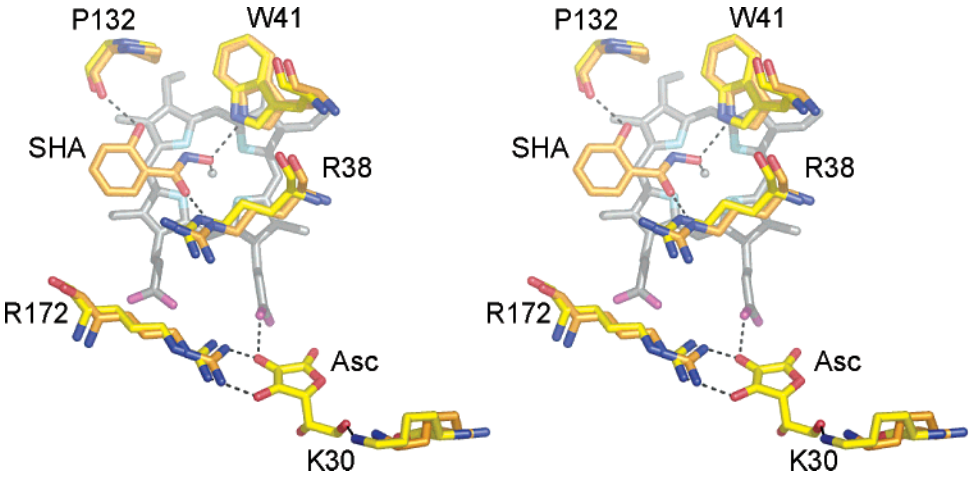

FIGURE 6: Structure-based alignment of the rsAPX−ascorbate complex [yellow (*26*)] and the rsAPX−SHA complex (orange). The residues involved in binding of ascorbate (Arg172 and Lys30) and SHA (Pro132, Arg38, and Trp41) are shown in both cases. The heme is shown in gray in both cases. The two hemes directly superimpose (for clarity, only one heme is indicated). Hydrogen bonds are indicated by dashed lines (black). This figure was prepared using PyMOL (*50*).

defined by the loop incorporating Ala70, the turn including Asp133 and the region of Ser173, and the edge of the heme; these are highlighted in Figure 4. The polar side chains of Asp133 and Ser69 extend into the solvent region. In the rsAPX and rsAPX−ascorbate stuctures (*26*), the equivalent site is occupied by five well-ordered solvent atoms.

The detailed structure of the rsAPX−SHA complex in the region of the heme is shown in Figure 5. The phenolic group [pK_a = 7.4 (*33*); Figure 2] of the hydroxamic acid group is coordinated to the heme iron at a distance of 2.1 Å, which is consistent with the electronic absorption spectra above. The SHA molecule is also able to hydrogen bond to the indole nitrogen of Trp41 (Figure 5). There are hydrogen bonds between the phenolic hydroxide [pK_a = 9.8 (*33*)] and the main chain carbonyl of Pro132, and between the carbonyl oxygen of SHA and the side chain guanadinium group of

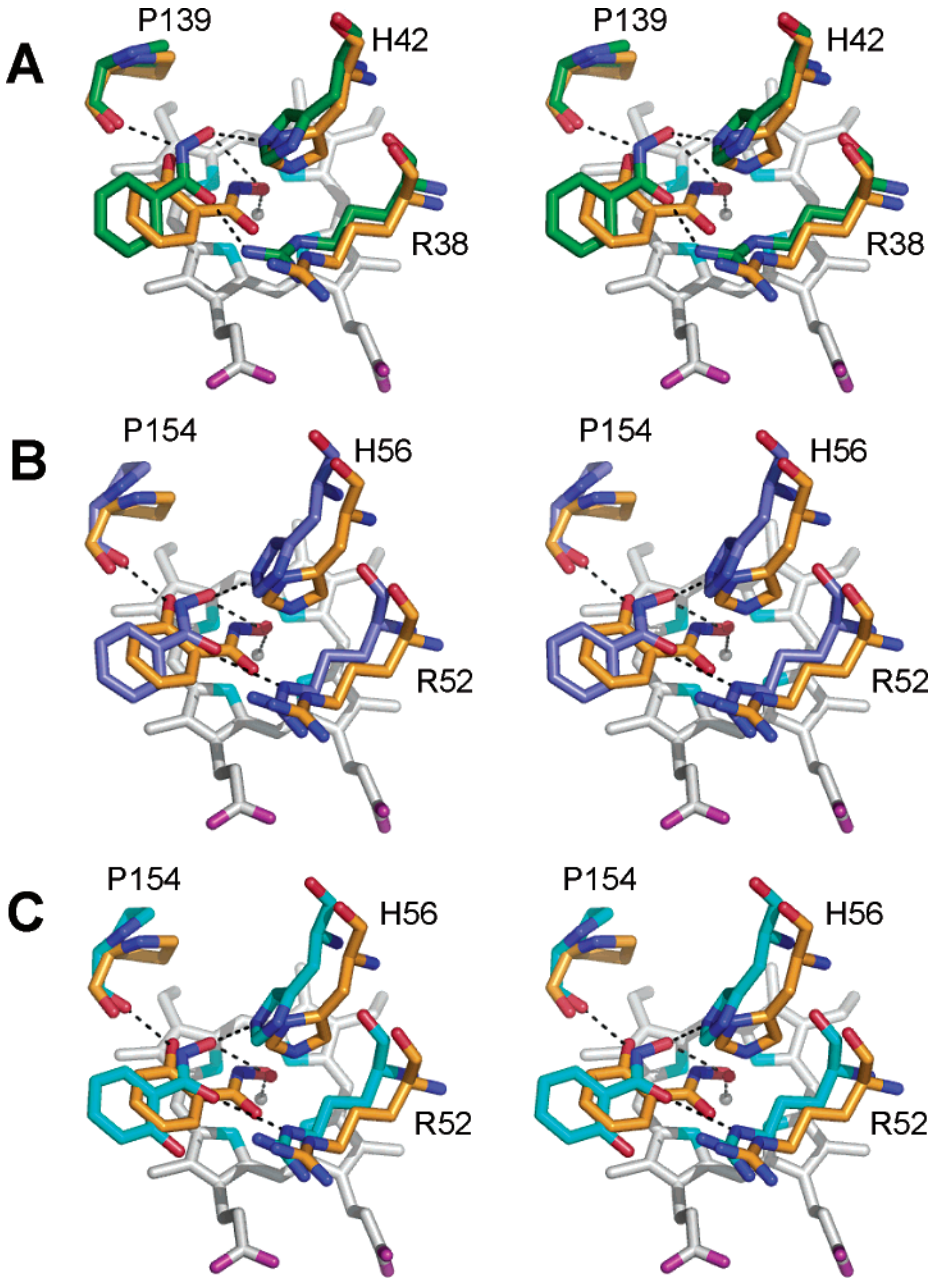

FIGURE 7: Structure-based alignments of the rsAPX−SHA complex (orange) and (A) the HRP−BHA complex (dark green; *13*), (B) the ARP−BHA complex (blue; *15*), and (C) the ARP−SHA complex (light blue; *38*). The residues involved in binding of the substrate for the HRP (Pro139, His42, and Arg38) and ARP (Pro154, His56, and Arg52) structures are overlaid with the corresponding residues in the rsAPX−SHA structure (Pro132, His42, and Arg38, respectively). The heme is shown in gray, and the two hemes directly superimpose in all cases; for clarity, only one heme is indicated. Hydrogen bonds for the HRP−BHA, ARP−BHA, and ARP−SHA structures are represented by dashed lines (black); hydrogen bonds for the rsAPX−SHA complex are omitted for clarity, but are according to Figure 6. This figure was prepared using PyMOL (*50*).

Arg38 (Figure 5). Pro132 and Arg38 are conserved in all APXs examined so far (*36*) as well as in other peroxidases (*5*). Trp41 is conserved in all but two APXs (*Mesembryanthemum crystallinum* APX and a membrane-bound enzyme from spinach which contain Phe at this position[3]). Although Nϵ of the distal histidine (His42) is 3.0 Å from the phenolic oxygen of SHA, the geometry is poor for formation of a hydrogen bond between His42 and SHA. The aromatic ring of the SHA molecule is almost parallel to the heme (separation of 3.4 Å) and makes a shallow angle of ~15° with the plane of the heme, and it overlaps with the δ-heme edge (C20 position) and the 8-Me group of the heme. The Cα and Cβ atoms of Ala70 are within van der Waals distance of the SHA (≈3.5 Å, Figure 4). Figure 6 shows an overlay of the rsAPX−ascorbate (*26*) and rsAPX−SHA structures; this clearly highlights the different binding locations of the SHA and ascorbate close to the δ- and γ-heme edge, respectively.

DISCUSSION

The identification of an ascorbate binding site close to the γ-heme edge (*26*) was counter to established thinking in

[3] In addition, these are also the only APXs examined so far that do not contain Trp at position 179 (replaced with Phe); they also lack one of the residues required for ascorbate binding (R172 → Ile for *M. crystallinum* and K30 → D for the spinach enzyme).

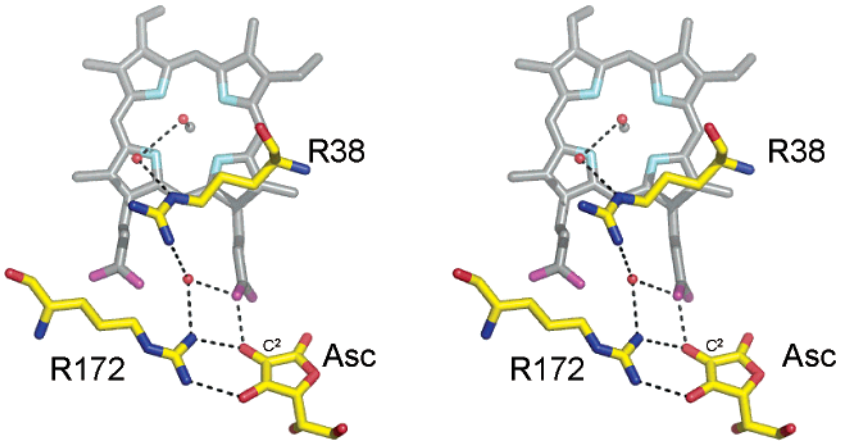

FIGURE 8: Proposed proton transfer pathway using Arg38. Water molecules are shown as red spheres, and hydrogen bonds are represented by dashed lines. The OH group on C^2 of ascorbate (Figure 2) is indicated. This figure was prepared using PyMOL (*50*).

which substrate binding and oxidation at the δ-heme edge had been widely assumed. However, most APXs that have been identified so far are also functionally competent for oxidation of aromatic substrates, and in some cases, oxidation of aromatic substrates occurs at a rate comparable to the rate of oxidation of ascorbate itself (*18*, *22*). The identity of this second substrate binding location was not known, but the region close to the δ-heme edge has been directly implicated (*23*, *24*).

The data presented in this work now complete the structural definition of the two binding sites in APX and confirm the δ-heme edge as the binding site for aromatic molecules. The structure is consistent with our steady-state data that show that APX modified at the δ-heme edge using phenylhydrazine retains ≈10% activity with ascorbate but is inactive against guaiacol (data not shown). The structure also provides rationalization of the empirical observation (*37*) that salicylic acid (2-hydroxybenzoic acid, Figure 2) is a (slow) substrate for APX with a possible role *in planta*. For salicylic acid, coordination to the iron is not observed (*37*) but the main hydrogen bonding interactions between Pro132 and Arg38 (Figure 5) are still possible.

Comparison with Other Peroxidases. In the following discussion, we correlate these structural data with our current understanding of substrate binding and oxidation in other class I, class II, and class III peroxidase enzymes. In Figure 7, we compare the rsAPX−SHA structure with the structures of the HRP−BHA complex (*13*) (Figure 7A), the ARP−BHA complex (*15*) (Figure 7B), and the ARP−SHA complex (*38*) (Figure 7C). It is clear from Figure 7 that the binding location of the substrate for all the structures is similar and close to the δ-heme edge. (We note also that oxidation of guaiacol has been reported to be inhibited by the presence of BHA (*21*), indicating that BHA also binds at the same δ-heme site in APX.) In all cases, there are hydrogen bonding interactions between the backbone carbonyl of a proline and between the distal arginine residue and the carbonyl of the BHA or SHA molecule; the distal histidine hydrogen bonds to the substrate in the HRP and ARP structures, but not in rsAPX.[4] There are other differences. For the HRP and ARP structures, the interaction with the heme iron is via a water molecule (compared to through the hydroxyl group of the SHA in rsAPX) and the proline carbonyl interacts with the NH group of the hydroxamic group (compared to the phenolic group of SHA in rsAPX). Altogether, the bound ligand for the HRP and ARP structures is displaced by approximately a bond length from the binding pocket relative to SHA in rsAPX. It is possible that the additional hydrogen bonding interaction between SHA and Trp41 in rsAPX (Figure 5) is partly responsible for this difference (Trp41 is replaced with a Phe in both HRP and ARP).

Might this binding site be used more generally for oxidation of related aromatic substrates in other class I peroxidases? Cytochrome *c* peroxidase is known (*39*) to bind aromatic substrates at a different location compared to cytochrome *c* (*40*), and the δ-meso heme edge has been implicated (*40*, *41*). This is consistent with our data because the key hydrogen-bonding residues (Arg38, Trp41, and Pro132) are conserved in CcP (Arg48, Trp51, and Pro145, respectively) and because CcP contains a similar binding pocket as identified in APX.

Mechanistic and Functional Implications. In light of these new data, and with the location of both the ascorbate (*26*) and aromatic binding sites in APX now defined, it is appropriate to correlate the new structural information with functional data and to consider the broader mechanistic question of how APX might most effectively deal with oxidation of different types of substrates bound at different locations. For ascorbate oxidation, our data (*26*) show direct coupling of the heme to the substrate through the 6-propionate and electron transfer to the heme is presumed to be facile. The data presented in this work show SHA to be in van der Waals contact with the porphyrin π-system, and for aromatic substrates, we therefore assume that electron transfer is directly through the π-orbitals of the porphyrin. Reduction of both Compound I and Compound II by both ascorbate (at the γ-heme edge) and aromatic substrates (at the δ-heme edge) also requires proton transfer (eqs 1−3); however, the mechanism of proton transfer is not well-developed for any heme peroxidase, and there is no information at all for APX. For ascorbate, oxidation of the (anionic, Figure 2) substrate gives the protonated monodehydroascorbate radical which is very acidic [$pK_a = -0.45$ for C^2-OH

[4] The distal histidine and arginine groups, and the main chain carbonyl of proline, are also involved in binding of ferulic acid to HRP (*14*).

(*42*, *43*); Figure 2] and will rapidly deprotonate. A proton transfer pathway from the ascorbate to a water molecule bound to the heme iron is identified that involves Arg38 (Figure 8). (Proton transfer to His42 may subsequently occur in solution, but the crystallographic data do not show a good hydrogen bonding interaction between this water and His42.) This distal arginine residue, which is known to be mobile in CcP (*44*−*47*) and which is conserved across all peroxidases (*5*), is also involved in binding of SHA in rsAPX (Figure 7), so might this residue also provide a conduit for proton delivery for aromatic substrates bound at the *δ*-heme edge, thereby providing APX with a common mechanism for proton shuttling during oxidation of both types of substrates? Clearly, this has yet to tested experimentally, but it would be consistent with the idea that APX is a hybrid enzyme that combines features that are characteristic of both class I and class III peroxidases (*21*) and with the suggestion that Arg38 in HRP is involved in proton transfer during oxidation of ferulic acid (*14*).

ACKNOWLEDGMENT

We thank Dr. David Leys for collection of crystallographic data. Mr. K. Singh is gratefully acknowledged for technical assistance.

REFERENCES

1. Everse, J., Everse, K. E., and Grisham, M. B. (1991) *Peroxidases in Chemistry and Biology*, Vols. I and II, CRC Press, Boca Raton, FL.
2. English, A. M., and Tsaprailis, G. (1995) Catalytic structure−function relationships in heme peroxidases, *Adv. Inorg. Chem. 43*, 79−125.
3. Veitch, N. C., and Smith, A. T. (2001) Horseradish peroxidase, *Adv. Inorg. Chem. 51*, 107−162.
4. Dunford, H. B. (1999) *Heme Peroxidases*, John Wiley, Chichester, U.K.
5. Welinder, K. G. (1992) Superfamily of plant, fungal and bacterial peroxidases, *Curr. Opin. Chem. Biol. 2*, 388−393.
6. Erman, J. E., and Vitello, L. B. (2002) Yeast cytochrome *c* peroxidase: mechanistic studies via protein engineering, *Biochim. Biophys. Acta 1597*, 193−220.
7. Smith, A. T., and Veitch, N. C. (1998) Substrate binding and catalysis in heme peroxidases, *Curr. Opin. Chem. Biol. 2*, 269−278.
8. Erman, J. E. (1998) Cytochrome *c* peroxidase: a model heme protein, *J. Biochem. Mol. Biol. 31*, 307−327.
9. Pelletier, H., and Kraut, J. (1992) Crystal structure of a complex between electron transfer partners, cytochrome *c* peroxidase and cytochrome *c*, *Science 258*, 1748−1755.
10. Davey, C. A., and Fenna, R. E. (1996) 2.3 Å resolution X-ray crystal structure of the bisubstrate analague inhibitor salicylhydroxamic acid bound to human myeloperoxidase, *Biochemistry 35*, 10967−10973.
11. Meno, K., Jennings, S., Smith, A. T., Henricksen, A., and Gajhede, M. (2002) Structural analysis of the two horseradish peroxidase catalytic residue variants H42E and R38S/H42E: implications for the catalytic cycle, *Acta Crystallogr. D58*, 1803−1812.
12. Sundaramoorthy, M., Kishi, K., Gold, M. H., and Poulos, T. L. (1994) The crystal structure of manganase peroxidase from *Phanerochaete crysosporium* at 2.06 Å resolution, *J. Biol. Chem. 269*, 32759−32767.
13. Henriksen, A., Schuller, D. J., Meno, K., Welinder, K. G., Smith, A. T., and Gajhede, M. (1998) Structural interactions between horseradish peroxidase C and the substrate benzhydroxamic acid determined by X-ray crystallography, *Biochemistry 37*, 8054−8060.
14. Henriksen, A., Smith, A. T., and Gajhede, M. (1999) The structures of the horseradish peroxidase C-ferulic acid complex and the ternary complex with cyanide suggest how peroxidases oxidise small phenolic substrates, *J. Biol. Chem. 274*, 35005−35011.
15. Itakura, H., Oda, Y., and Fukuyama, K. (1997) Binding mode of benzhydroxamic to *Arthromyces ramosus* peroxidase shown by X-ray crystallographic analysis of the complex at 1.6 Å resolution, *FEBS Lett. 412*, 107−110.
16. Fiedler, T. J., Davey, C. A., and Fenna, R. E. (2000) X-ray crystal structure and characterisation of halide-binding sites of human myeloperoxidase at 1.8 Å resolution, *J. Biol. Chem. 275*, 11964−11971.
17. Fukuyama, K., Sato, K., Itakura, H., Takahashi, S., and Hosoya, T. (1997) Binding of iodide to *Arthromyces ramosus* peroxidase investigated with X-ray crystallographic analysis, ^{1}H and ^{127}I NMR spectroscopy and steady state kinetics, *J. Biol. Chem. 272*, 5752−5756.
18. Raven, E. L. (2003) Understanding functional diversity and substrate specificity in haem peroxidases: what can we learn from ascorbate peroxidase? *Nat. Prod. Rep. 20*, 367−381.
19. Sharp, K. H., Moody, P. C. E., and Raven, E. L. (2003) Defining substrate specificity in haem peroxidases, *Dalton Trans.*, 4208−4215.
20. Dalton, D. A. (1991) Ascorbate peroxidase, in *Peroxidases in Chemistry and Biology* (Everse, J., Everse, K. E., and Grisham, M. B., Eds.) pp 139−154, CRC Press, Boca Raton, FL.
21. Heering, H. A., Jansen, M. A. K., Thorneley, R. N. F., and Smulevich, G. (2001) Cationic asorbate peroxidase isozyme II from tea: structural insights into the heme pocket of a unique hybrid peroxidase, *Biochemistry 40*, 10360−10370.
22. Raven, E. L. (2000) Peroxidase-catalysed oxidation of ascorbate: structural, spectroscopic and mechanistic correlations in ascorbate peroxidase, in *Subcellular Biochemistry: Enzyme Catalysed Electron and Radical Transfer* (Holzenberg, A., and Scrutton, N. S., Eds.) Kluwer Academic/Plenum Publishers: New York pp 318−350.
23. Mandelman, D., Jamal, J., and Poulos, T. L. (1998) Identification of two-electron-transfer sites in ascorbate peroxidase using chemical modification, enzyme kinetics, and crystallography, *Biochemistry 37*, 17610−17617.
24. Hill, A. P., Modi, S., Sutcliffe, M. J., Turner, D. D., Gilfoyle, D. J., Smith, A. T., Tam, B. M., and Lloyd, E. (1997) Chemical, spectroscopic and structural investigation of the substrate-binding site in ascorbate peroxidase, *Eur. J. Biochem. 248*, 347−354.
25. Bursey, E. H., and Poulos, T. L. (2000) Two substrate binding sites in ascorbate peroxidase: the role of arginine 172, *Biochemistry 39*, 7374−7379.
26. Sharp, K. H., Mewies, M., Moody, P. C. E., and Raven, E. L. (2003) The crystal structure of the ascorbate peroxidase/ascorbate complex, *Nat. Struct. Biol. 10*, 303−307.
27. Lad, L., Mewies, M., and Raven, E. L. (2002) Substrate binding and catalytic mechanism in ascorbate peroxidase: evidence for two ascorbate binding sites, *Biochemistry 41*, 13774−13781.
28. Santimone, M. (1975) Titration study of guaiacol oxidation by horseradish peroxidase, *Can. J. Biochem. 53*, 649−657.
29. Bogumil, R., Hunter, C. L., Maurus, R., Tang, H.-L., Lee, H., Lloyd, E., Brayer, G. D., Smith, M., and Mauk, A. G. (1994) FTIR analysis of the interaction of azide with horse heart myoglobin mutants, *Biochemistry 33*, 7600.
30. Aitken, S. M., Turnbull, J. L., Percival, M. D., and English, A. M. (2001) Thermodynamic analysis of the binding of aromatic hydroxamic acid analogues to ferric horseradish peroxidase, *Biochemistry 40*, 13980−13989.
31. Indiana, C., Santoni, E., Becucci, M., Boffi, A., Fukuyama, K., and Smulevich, G. (2003) New insight into the peroxidase-hydroxamic acid interactions revealed by the combination of spectroscopic and crystallographic studies, *Biochemistry 42*, 14066−14074.
32. Schonbaum, G. R. (1973) New complxes of peroxidases with hydroxamic acids, hydrzides and amides, *J. Biol. Chem. 248*, 502−511.
33. O'Brien, E. C. O., Farkas, E., Gil, M. J., Fitzgerald, D., Castineras, A., and Nolan, K. B. (2000) Metal complexes of salicylhydroxamic acid (H_2SHA), anthranilic hydroxamic acid and benzohydroxamic acid. Crystal and molecular structure of $[Cu(phen)_2Cl]Cl.\ H_2SHA$, a model for a peroxidase-inhibitor complex, *J. Inorg. Biochem. 79*, 47−51.
34. Collaborative Computational Project No. 4 (1994) The *CCP*4 suite: programs for protein crystallography, *Acta Crystallogr. D50*, 760−763.
35. McRee, D. (1992) A Visual Protein Crystallographic Software System for X11/Xview, *J. Mol. Graphics 10*, 44−47.

36. Jespersen, H. M., Kjaersgard, I. V. H., Ostergaard, L., and Welinder, K. G. (1997) From sequence analysis of three novel ascorbate peroxidases from *Arabidopsis thaliana* to structure, function and evolution of seven types of ascorbate peroxidase, *Eur. J. Biochem. 326*, 305−310.
37. Kvaratskhelia, M., George, S. J., and Thorneley, R. N. F. (1997) Salicylic acid is a reducing substrate and not an effective inhibitor of ascorbate peroxidase, *J. Biol. Chem. 272*, 20998−21001.
38. Tsukamoto, K., Itakura, H., Sato, K., Fukuyama, K., Miura, S., Takahashi, S., Ikezawa, H., and Hosoya, T. (1999) Binding of salicylahydroxamic acid and several aromatic donor molecules to *Arthromyces ramosus* peroxidase, investigated by X-ray crystallography, optical difference spectroscopy and NMR relaxation, molecular dynamics and kinetics, *Biochemistry 38*, 12558−12568.
39. Yonetani, T., and Ray, G. S. (1965) Studies on cytochrome *c* peroxidase. Purification and some properties, *J. Biol. Chem. 240*, 4503−4514.
40. DePillis, G. D., Sishta, B. P., Mauk, A. G., and Ortiz de Montellano, P. R. (1991) Small substrates and cytochrome *c* are oxidized at different sites of cytochrome *c* peroxidase, *J. Biol. Chem. 266*, 19334−19341.
41. Wilcox, S. K., Jensen, G. M., Fitzgerald, M. M., McRee, D. E., and Goodin, D. B. (1996) Altering substrate specificity at the heme edge of cytochrome *c* peroxidase, *Biochemistry 35*, 4858−4866.
42. Bryan, D. M., Dell, S. D., Kumar, R., Clarke, M. J., Rodriguez, V., Sherban, M., and Charkoudian, J. (1988) Stable pentaammineruthenium(III) complexes of reductic acids: synthesis, linkage isomers and autoxidation kinetics, *J. Am. Chem. Soc. 110*, 1498−1506.
43. Creutz, C. (1981) The complexities of ascorbate as a reducing agent, *Inorg. Chem. 20*, 4452−4453.
44. Bonagura, C. A., Bhaskar, B., Shimizu, H., Li, H., Sundaramoorthy, M., McRee, D. E., Goodin, D. B., and Poulos, T. L. (2003) High-resolution crystal structures and spectroscopy of native and Compound I cytochrome *c* peroxidase, *Biochemistry 42*, 5600−5608.
45. Edwards, S. L., Poulos, T. L., and Kraut, J. (1984) The crystal structure of fluoride-inhibited cytochrome *c* peroxidase, *J. Biol. Chem. 259*, 12984−12988.
46. Edwards, S. L., Xuong, N., Hamlin, R. C., and Kraut, J. (1987) Crystal structure of cytochrome *c* peroxidase Compound I, *Biochemistry 26*, 1503−1511.
47. Fulop, V., Phizackerley, R. P., Soltis, S. M., Clifton, I. J., Wakatsuki, S., Erman, J., Hajdu, J., and Edwards, S. L. (1994) Laue diffraction study on the structure of cytochrome *c* peroxidase compound I, *Structure 2*, 201−208.
48. Kraulis, P. J. (1991) MOLSCRIPT: A program to produce both detailed and schematic plots of protein structures, *J. Appl. Crystallogr. 24*, 946−950.
49. Merrit, E. A., and Murphy, M. E. P. (1994) Raster3D Version 2.0: A program for photorealistic molecular graphics, *Acta Crystallogr. D50*, 869−873.
50. DeLano, W. L. (2002) The PyMOL Molecular Graphics System, DeLano Scientific, San Carlos, CA.
51. Berman, H. M., Westbrook, J., Feng, Z., Gilliland, G., Bhat, T. N., Weissig, H., Shindyalov, I. N., and Bourne, P. E. (2000) The Protein Data Bank. *Nucleic Acids Res. 28*, 235−242.

BI049343Q